DAMAGING CONFIGURATIONS IN ARCH STRUCTURES WITH VARIABLE CURVATURE AND TAPERED CROSS-SECTION

(Article begins on next page)

Damaging Configurations in Arch Structures with Variable Curvature and Tapered Cross-section

Jonathan Melchiorre, Amadeo Manuello, Laura Sardone, Giuseppe Carlo Marano

DAMAGING CONFIGURATIONS IN ARCH STRUCTURES WITH VARIABLE CURVATURE AND TAPERED CROSS-SECTION

Jonathan Melchiorre[1]*, Amedeo Manuello[1], Laura Sardone[2], and Giuseppe Carlo Marano[1]

[1] Department of Structural, Geotechnical and Building Engineering Politecnico di Torino, Corso Duca degli Abruzzi, 24 - 10129. Torino, Italy.
[2] Department of Civil Engineering and Architecture Sciences. Politecnico di Bari, Via Edoardo Orabona, 4 – 70126. Bari, Italy.
*Corresponding author E-mail: jonathan.melchiorre@polito.it

Key words: Arch structures, Damaging in Arch, Structural Design, Conceptual Design, Damaged Arch Structures, Variable Curvature, Tapered Cross-section

Abstract. *Arch structure is a widely used and important structure type all over the World. Due to its beautiful form and large spanning capacity, arch structure is widely used in bridges, tunnels and other buildings. Recently, the large span space arch structure has a stage of development. The defects of arch structure, such as connection, material, fatigue, stress concentration and welding, will directly affect the safety of these kind of structures. The study of the evolution of the damage in arches is a topic of interest since the antiquity. A well-done structural design should always account for the evolution of the damage in time, in particular if it can bring to a change in the static behaviour of the structure itself under different loading conditions. In this paper, a model for the calculation of localized damaged in arch structures is presented. In particular, using an analytical solution for the computation of the displacements field and the consequent internal actions of very general shapes with variable curvature and tapered cross-section, the damage is modelled by localized depletion of the cross-sectional properties (inertia) in the different points along the arch axis. Moreover, the depleted parameters are the cross-section and the bending stiffness of the arch. The model is applied to the study different configurations of the damage (localization of plastic hinges or different pattern of defects) and to consider the evolution of the damage in time.*

1 INTRODUCTION

The arch shape has been used since ancient times to make structures that can effectively withstand applied loads. Nowadays, this type of structure is mainly used to support long-span structures with special reference to road and rail bridges and large roofs. In particular, the use of structural steel, since the last century, has made it possible to build longer and longer span arches thanks to the mechanical properties of this material which, nowadays, is used in a great many fields of structural engineering. In recent years, rising costs and the environmental impact associated with the unrestrained use of steel in civil engineering have directed research toward finding optimized structural shapes and geometries that are able to make the most of the material's mechanical properties so as to reduce the amount employed [1–20]. This has led to an ever-increasing exploitation of the strength of construction materials and the exploration of their limits even in the nonlinear field. In particular, many studies have been conducted to understand the phenomena of structural instability [21–25] and to understand how structure damage

1

can evolve as a function of time and applied loads [26]. For this purpose, various studies for the damage detection [27–30] and modelling have been realized for each type of structure and material [31–33]. In this paper, a model is presented to study the evolution of damage due to increasing overloads on steel arches with a variable radius of curvature and tapered cross-section. In Section 2, the method for calculating stresses and identifying damaged arch sections is explained. This methodology is based on solving a sixth-order differential equation by the finite difference method. The proposed solution was implemented in a self-made code developed in Matlab [34]. At the end of the Section, the presented method is validated through a comparison of results with those obtained by means of the computational software SAP2000 [35], based on the finite element method. Finally, in Section 3, the proposed method is applied to two different steel parabolic arches of different geometry, so that it is possible to study how different geometries can give rise to different damage patterns.

2 METHODOLOGY

In this study, an original analytical-numerical methodology for the analysis of arches with very generic geometry is utilized to analyze the evolution of damage configurations of arch structures subjected to increasing overloads. This method allows the calculation of internal actions, displacements, rotations and stresses of arches with variable curvature radius and tapered cross-section. These quantities are calculated using a sixth-order differential equation that allows the tangential displacements u to be obtained as a function of the curvilinear abscissa s. The equation can be obtained by considering the static, kinematic and constitutive equations [36] for a generic curved beam considering the assumption of negligible beam elongation $\varepsilon = 0$ and shear strain $\gamma = 0$. Under these assumptions, a sixth-order differential equation was calculated in the following form:

$$au^{(6)} + bu^{(5)} + cu^{(4)} + du^{(3)} + eu^{(2)} + fu^{(1)} + gu + h = 0 \tag{1}$$

Where Lagrange's notation is used for derivatives, hence $u^{(d)}$ is the d-th order derivative of the function u, that represents the displacements in the tangential direction, with respect to the curvilinear abscissa s. The functions $a, ..., g$ are expressed in terms of the functions defined in Table 1, where R is the curvature radius of the arch and J is the bending inertia of the cross-section. In particular, considering C the generic function of the set $\{a, ..., g\}$ and by C_d, $d = 0, ..., 3$, the corresponding functions in Table 1, the generic expression for $a, ..., g$ is

$$C = \left(RJ^{(3)} + R^{(1)}J^{(2)} + \frac{1}{R}J^{(1)}\right)C_0 + \left(3RJ^{(2)} + 2R^{(1)}J^{(1)} + \frac{1}{R}J\right)C_1 +$$
$$+ \left(3RJ^{(1)} + R^{(1)}J^{(1)}\right)C_2 + RJC_3 \tag{2}$$

Finally, the function h used in equation (1) is

$$h = \frac{1}{E}\left(P_t + R^{(1)}P_n + RP_n^{(1)} - \frac{m}{R} - R^{(1)}m^{(1)} - Rm^{(2)}\right) \tag{3}$$

Where E is the Young's Modulus of the material and the functions P_n, P_t and m are the external load applied to the structure and, respectively they represent the external force normal to the arch, the external force tangent to the arch and the external applied bending moment, e.g. see Figure 1.

Being the Equation (1) a sixth order differential equation, a determined solution can be obtained only by considering six boundary conditions. In this paper, the focus is on two types of static scheme: fully

$a_0 = 0$	$b_0 = 0$
$a_1 = 0$	$b_1 = 0$
$a_2 = 0$	$b_2 = R$
$a_3 = R$	$b_3 = 5R^{(1)}$
$c_0 = 0$	$d_0 = R$
$c_1 = R$	$d_1 = 3R^{(1)}$
$c_2 = 4R^{(1)}$	$d_2 = 6R^{(2)} + \dfrac{1}{R}$
$c_3 = 10R^{(2)} + \dfrac{1}{R}$	$d_3 = 10R^{(3)} - 4R^{(1)}\dfrac{1}{R^2}$
$e_0 = 2R^{(1)}$	$f_0 = R^{(2)} + \dfrac{1}{R}$
$e_1 = 3R^{(2)} + \dfrac{1}{R}$	$f_1 = R^{(3)} - 2R^{(1)}\dfrac{1}{R^2}$
$e_2 = 4R^{(3)} - 3R^{(1)}\dfrac{1}{R^2}$	$f_2 = R^{(4)} - 3R^{(2)}\dfrac{1}{R^2} + 6(R^{(1)})^2\dfrac{1}{R^3}$
$e_3 = 5R^{(4)} - 6R^{(2)}\dfrac{1}{R^2} + 12(R^{(1)})^2\dfrac{1}{R^3}$	$f_3 = R^{(5)} - 4R^{(3)}\dfrac{1}{R^2} + 24R^{(1)}R^{(2)}\dfrac{1}{R^3} - 24(R^{(1)})^3\dfrac{1}{R^4}$
$g_0 = -R^{(1)}\dfrac{1}{R^2}$	
$g_2 = -R^{(2)}\dfrac{1}{R^2} + 2(R^{(1)})^2\dfrac{1}{R^3}$	
$g_2 = -R^{(3)}\dfrac{1}{R^2} + 6R^{(1)}R^{(2)}\dfrac{1}{R^3} - 6(R^{(1)})^3\dfrac{1}{R^4}$	
$g_3 = -R^{(4)}\dfrac{1}{R^2} + 8R^{(1)}R^{(3)}\dfrac{1}{R^3} + 6(R^{(2)})^2\dfrac{1}{R^3} - 36(R^{(1)})^2R^{(2)}\dfrac{1}{R^4} + 24(R^{(1)})^4\dfrac{1}{R^5}$	

Table 1: Functions used to define the Equation (1).

restrained arch and hinged arch. In the case of fully restrained structure, the displacements u and v and the rotations φ are not allowed at the boundaries.

While, in the case of hinged arch, the rotations are allowed in the extremities but the bending moment should be null.

The solution of the Equation (1), together with the boundary conditions, is computed by a self-made code based on the finite difference method developed in Matlab [34]. Once the tangential displacements u have been calculated, the displacements in the normal direction v and the rotations φ can be obtained, as in Figure 1, by means of the following equations:

$$v = -Ru^{(1)} \tag{4}$$

$$\varphi = -Ru^{(2)} - R^{(1)}u^{(1)} - \frac{1}{R}u \tag{5}$$

Considering the static equations for a planar curved beam together with the Equations (4) and (5), it is possible to retrieve the beam deformation by the elastic curvature χ only, that results:
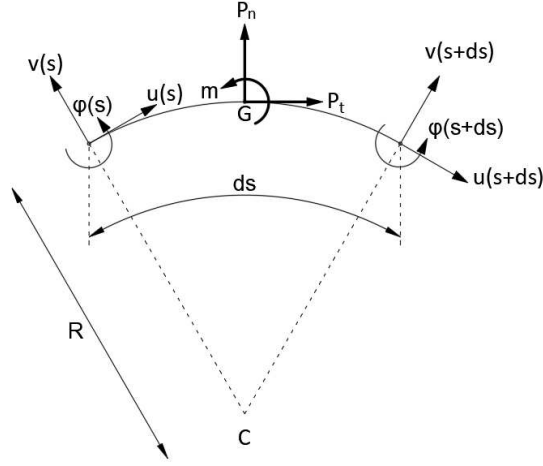
$$\chi = -Ru^{(3)} - 2R^{(1)}u^{(2)} - \left[R^{(2)} + \frac{1}{R}\right]u^{(1)} + \frac{R^{(1)}}{R^2}u \tag{6}$$

Finally, the applied bending moment M, the shear force V and the axial force N can be computed as follows:

$$M = EJ\chi \tag{7}$$

$$V = -M^{(1)} - m \tag{8}$$

$$N = R\left(P_n - M^{(2)} - m^{(1)}\right) \tag{9}$$

Figure 1: Displacements induced by external forces on an infinitesimal beam segment

| Node 1	Node 2		Node 3
$u_1^I = 0$	$u_2^I = u_2^{II}$	$N_2^I = N_2^{II}$	$u_3^{II} = 0$
$v_1^I = 0$	$v_2^I = v_2^{II}$	$V_2^I = V_2^{II}$	$v_3^{II} = 0$
$\varphi_1^I = 0$	$M_2^I = k(\varphi_2^I - \varphi_2^{II})$	$M_2^I = M_2^{II}$	$\varphi_3^{II} = 0$

Table 2: Boundary conditions related to the static scheme represented in Figure 2.

The presented method is used to analyze arch structures subjected to self-weight q_{sw} and to an increasing overload q_0. For each step of load increase, the internal actions are calculated and used to obtain the maximum Von Mises stresses σ^{VM} acting on each cross-section of the structure. Then it is verified that the applied stress σ^{VM} is less than the yield strength of the material employed f_y. In case the verification is not passed in a cross section, it is assumed that the structure has been damaged in the corresponding area. At this point, the damage is introduced by considering reducing the bending stiffness in the damaged area of the structure. To model such structural behavior, a rotational elastic spring with stiffness of k is assumed to be introduced into the damaged section. Thus the structure is divided into two arches, each of which can be analyzed using a different Equation (1), considering six boundary conditions for each arch. The solution will then be obtained by solving a system of equations comprising the two equations (1) for each of the two arches plus twelve equations representing the boundary conditions. It is important to note that the problem cannot be decoupled because the boundary conditions at the elastic spring involve equalizing displacements and internal actions at that point of the two afferent structures.

In the figure 2 the example of static scheme of fully restrained arch with rotational hinge in the midspan is shown. The structure is subjected to self-weight load q_{sw} and an overload q_0 constant along the arch axis s. The boundary conditions related to this example are given in Table 2.

To validate the presented method, a parabolic arch with the static scheme presented in Figure 2 is compared with an equivalent finite element model made with the commercial calculation software SAP2000 [35], e.g. see Figure 3.

The analyzed structure has a length $L = 100m$ and a height at the mid-span $f = 30m$. It is found to be subject to an overload $q_0 = 100kN/m$ and a self-weight load q_{sw} calculated assuming that the
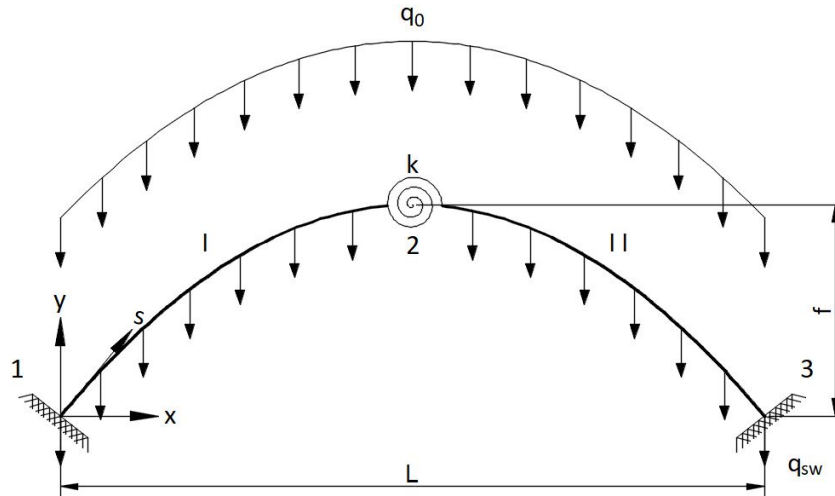
Figure 2: Static scheme of a fully restrained arch with a rotational hinge in the mid-span, subjected to self-weight load q_{sw} and an overload q_0

structure is composed entirely of structural steel type $S355$ which is found to have a weight per unit volume of $\gamma = 78.5 kN/m^3$. Furthermore, a hollow tubular cross-section was assumed whose dimensions vary with a quadratic law along the axis of the arch, being the radius of the cross-section at the base equal to $r_{base} = 0.50m$ and that of the cross-section at the mid-span equal to $r_{mid-span} = 0.25m$, while the thickness is considered constant $t = 0.05m$. Finally, an elastic constant of $k = 6615 kNm/rad$ was used for the rotational spring, which is proportional to $EJ/0.5L_{arch}$ where L_{arch} is the length of the arch. The results from the two analyses are compared in terms of displacements, rotations and internal actions and, as can be seen from the comparative graphs in Figure 4, the solutions turn out to be very similar. It should be noted that the small differences between the calculated quantities are due to the fact that the finite element model consists of straight segments with a constant cross section, being a simplified model of the case studied. The result obtained by the method presented in this paper is quite impressive as the case study examined has several critical issues, being an arch with variable radius of curvature and tapered cross section. Despite this, the calculated solution is very similar to that obtained with a validated software such as SAP2000 [35].
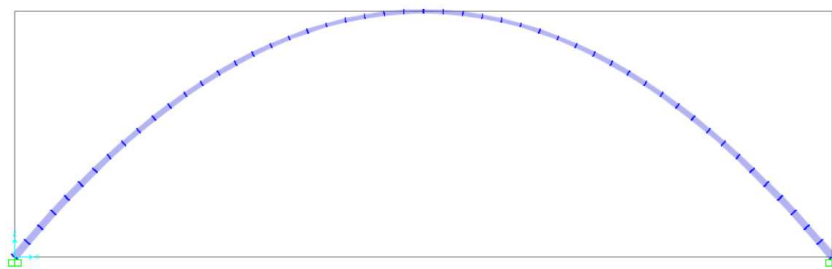
Figure 3: Finite element model made in SAP2000 of the arch used for the validation of the presented method.
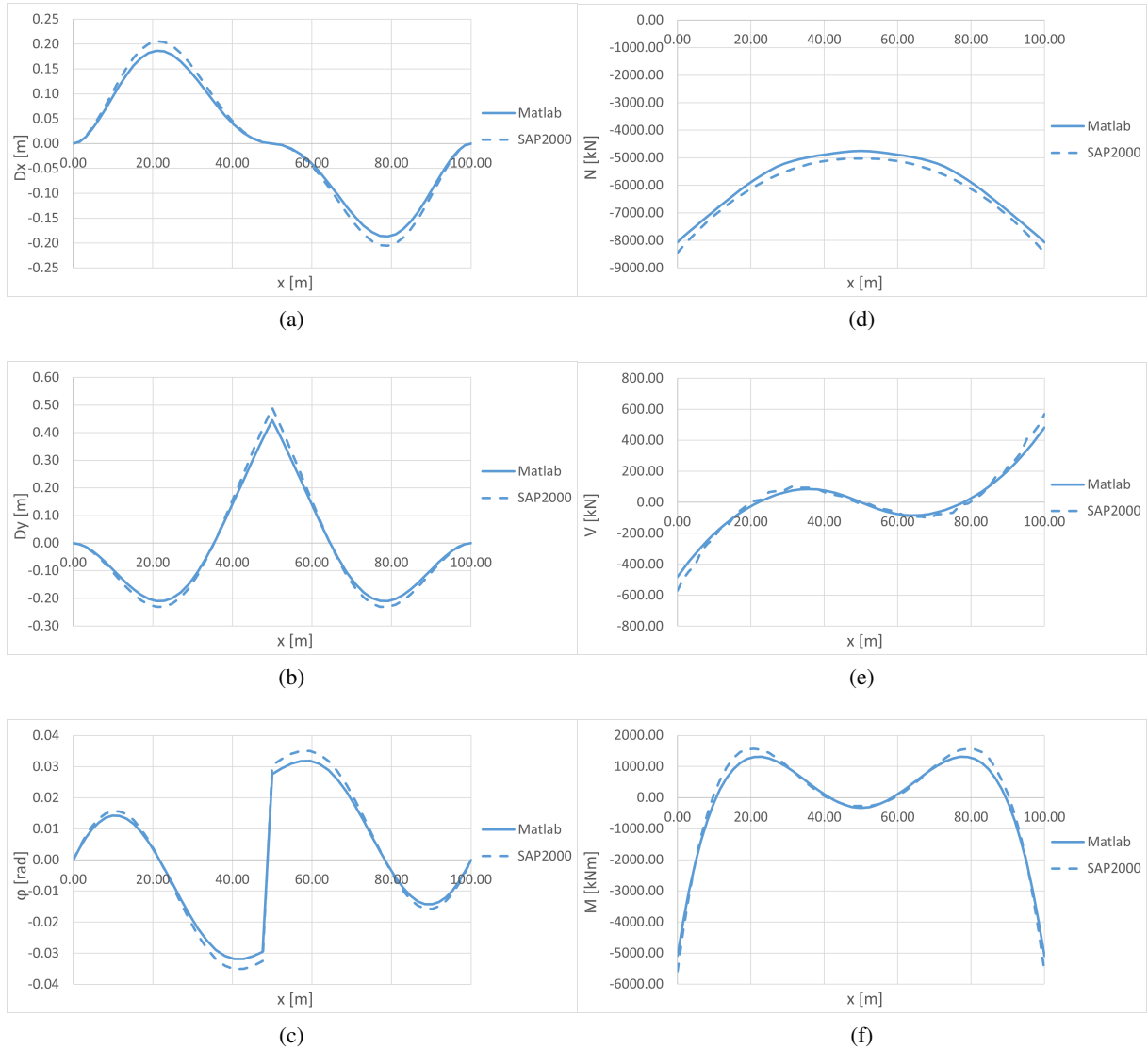
Figure 4: Analyses results comparison: Displacements in x-direction *Dx* (a), Displacements in y-direction *Dy* (b), Rotations φ (c), Axial Force *N* (d), Shear Force *V* (e), Bending Moment *M* (f).

3 RESULTS AND DISCUSSION

The method presented in Section 2 is used for the analysis of two geometric configurations of fully restrained parabolic arch structures in order to evaluate the evolution of damage and the change in the static scheme produced by the increasing overload. In particular, the arches studied are characterized by $L = 100m$ and $f = 30m$ and are both made of structural steel type $S355$ for which the yield stress is found to be $f_y = 355MPa$. The two structures studied are different because in the first case 3.1 is characterized by a constant cross-section along the axis of the arch, while in the second case 3.2 an arch with tapered cross-section is analyzed. It is important to note that only damage due to acting stresses was considered

in these simplified analyses, while global and local buckling effects are not taken into account.
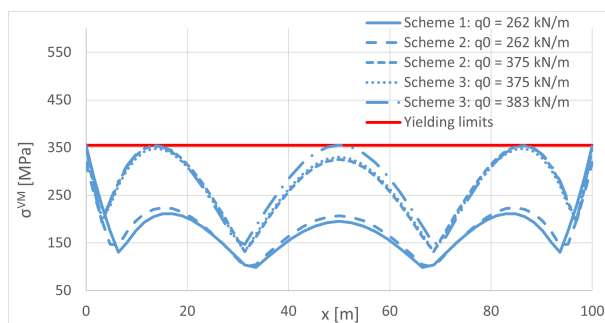

(a)

(b)
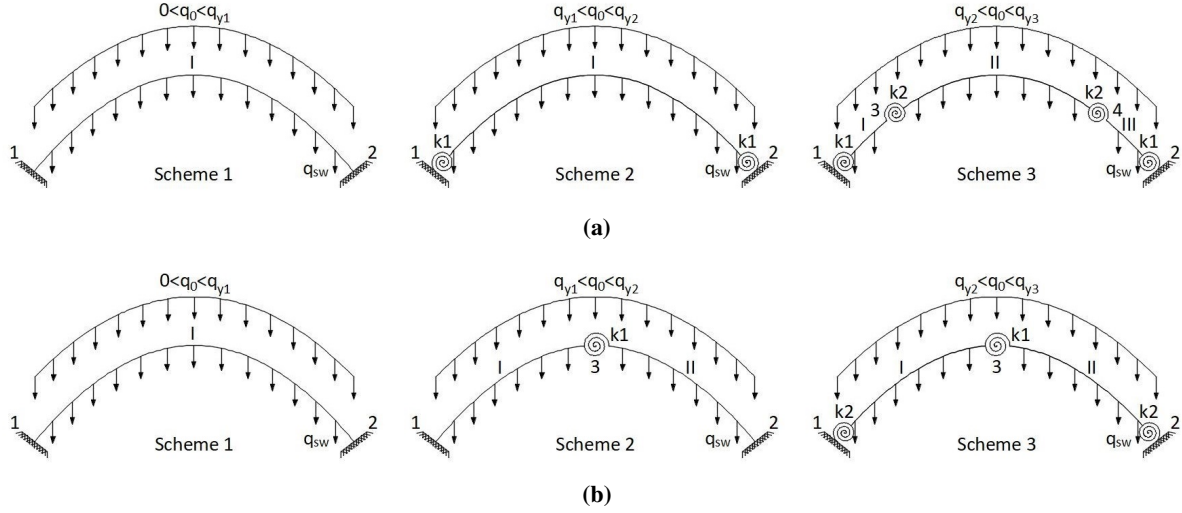
Figure 5: Evolution of damage due to an increasing overload: Arch with constant cross-section in Section 3.1 (a), Arch with tapered cross-section in Section 3.2 (b).

3.1 Fully restrained parabolic arch with constant cross-section

The first case analyzed is that of fully restrained arch with a constant tubular cross-section with radius $r = 0.50m$ and thickness $t = 0.05m$. The analysis is carried out by starting from the case of a structure subjected only to self-weight q_{sw} and then increasing the overload q_0 and performing tension verification for each new load increment. The process is iterated until at one or more points $\sigma^{VM} > f_y$ results. In this case, the structure is assumed to have been damaged in the yielded sections, and the damage is introduced into the model by going to insert elastic rotational springs of stiffness k at those specific points. After the change of static scheme, we continue to increase the applied overload while decreasing the rotational spring stiffness until new yielded cross-sections are identified. In particular, in the present case, the evolution of the static scheme is the one presented in Figure 5. The first failure occurs in the embedded cross-sections due to an overload $q_0 = q_{y1} = 262kn/m$. The base joints are then considered damaged and replaced with rotational elastic springs with stiffness $k1$ proportional to the material characteristics and cross-section properties. As a result of changing the static scheme, as expected, a redistribution of stresses in the structure (Figure 6) and an increase in displacements and rotations (Figure 8) are observed due to a decrease in structural stiffness.

Then continue to increase the overload and reduce the elastic stiffness of the springs at the base until different zones yield. In the present case, the new yielding is obtained for a load equal to $q_0 = q_{y2} = 375kN/m$ and an elastic stiffness $k1$ equal to 20% of the initial one. The resulting new static scheme will consist of four elastic springs, two at the base and two placed at a distance of about $15m$ from the supports. The new scheme, by appropriately reducing the elastic stiffness of the rotational springs, turns out to be able to withstand load increases up to $q_0 = q_{y3} = 383kN/m$.

Figure 6: Von Mises stresses applied to the arch with constant cross-section in Section 3.1

3.2 Fully restrained parabolic arch with tapered cross-section

The first case analyzed is that of fully restrained arch with a tapered tubular cross-section. The dimensions of the cross-sections vary with quadratic law along the arch axis, being the radius of the extremities cross-section $r_{base} = 0.50m$ and the radius of the mid-span cross-section $r_{mid-span} = 0.25m$, while the thickness remains constant for all the length of the structure $t = 0.05m$. Even in this case, the analysis is carried out by starting from the case of a structure subjected only to self-weight q_{sw} and then increasing the overload q_0 and performing tension verification for each new load increment. Having a tapered cross-section, in this case the first yielded cross-section is the one in the mid-span, that is the smaller one. This means that the damage configuration results to be totally different from the one in the previous case sudy, see Figure 5. The first failure occurs in the embedded cross-sections due to an overload $q_0 = q_{y1} = 195kn/m$. Then a rotational spring is used to replace the joint in the mid-span. Then, with a very small load increase, two more cross-sections will result damaged, the base ones. It is possible to notice that in this case $q_0 = q_{y2} = 199kn/m$ is very similar to q_{y1}, that means that the cross-section at the base will be damaged just after the reduction in stiffness in the mid-span. Finally, continuing to increase the overload and properly reducing the elastic stiffness of the springs, it is possible to find the failure load that results to be $q_{y3} = 213kN/m$. It is possible to notice that the final stress applied to the structure (Figure 7) is very similar to the one of the previous case (Figure 7). This means that with the increasing of the applied loads, the structures tends to similar tension configuration. Despite this, due to the lower stiffness of the tapered arch presented in Section 3.2, it can be seen in Figure 8 that the displacements and rotations are bigger than in the first case study.
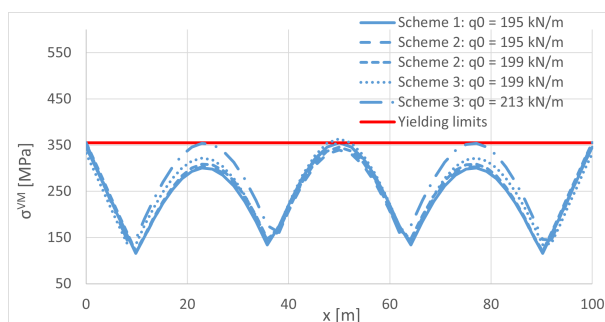
Figure 7: Von Mises stresses applied to the arch with tapered cross-section in Section 3.2

8
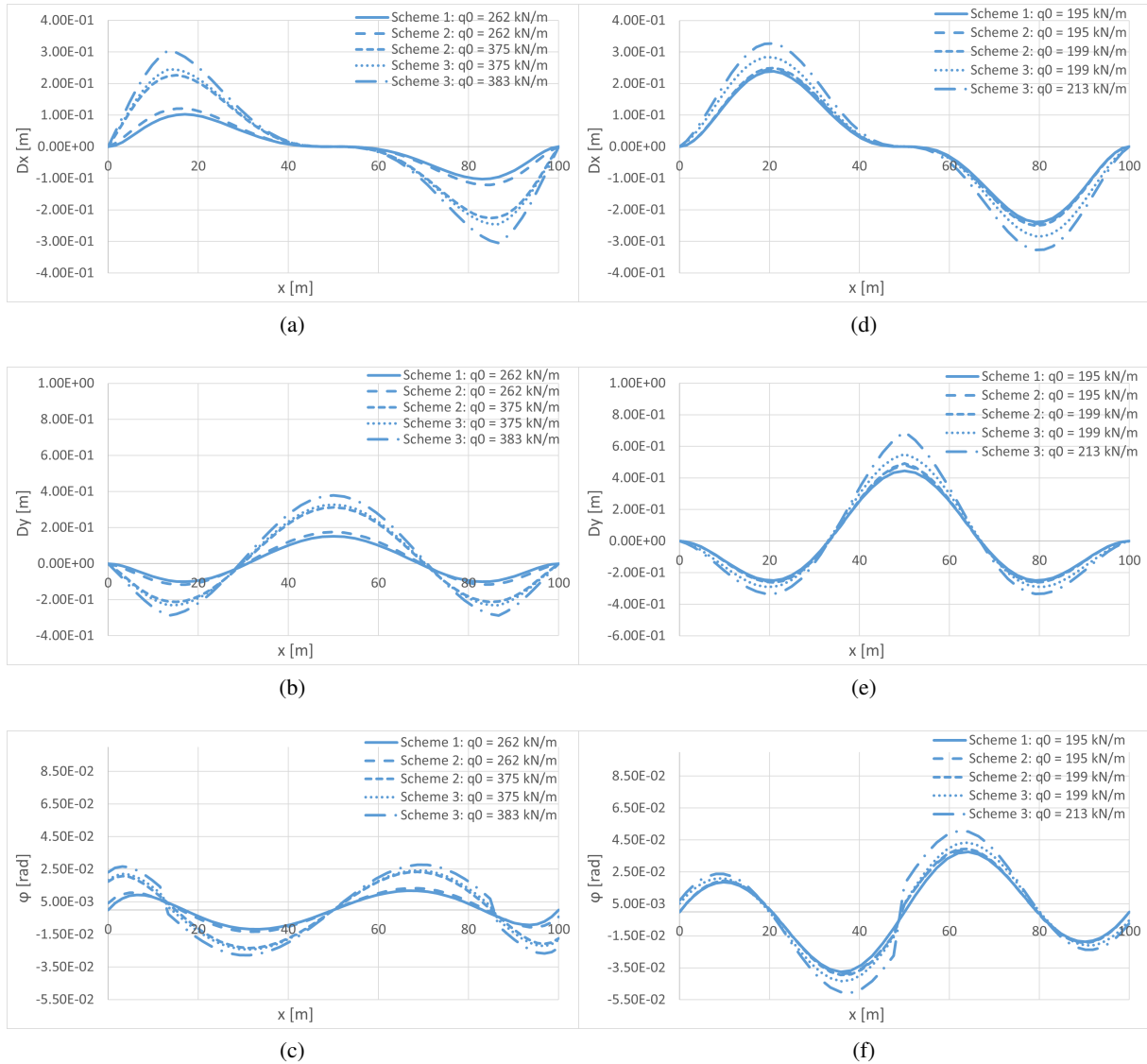
Figure 8: Analyses results comparison: Displacements in x-direction *Dx* (a), Displacements in y-direction *Dy* (b), Rotations φ (c), Axial Force *N* (d), Shear Force *V* (e), Bending Moment *M* (f).

4 CONCLUSIONS

In the current study, an analytical-numerical formulation for the calculation of curved beams with variable curvature radius and tapered cross-sections is presented. The method is used to calculate the Von Mises stresses applied to arch structures subjected to the self-weight and to an external overload. Then results are used to define the damaged zones of the structure. Finally, the damage is modeled as a reduction of concentrated stiffness by introducing elastic rotational spring in correspondence with the damaged cross-sections. The method is then implemented by a self-made code in Matlab [34] based on

the finite difference method. The validity of the procedure is proven by comparing the obtained results with ones calculated by commercial finite element based software, SAP2000 [35]. Finally, it is applied to two different arch configurations to study the evolution of the structural structural behaviour due to the damaged configurations caused by an increasing overload.

ACKNOWLEDGMENTS

REFERENCES

[1] Cucuzza, R., Rosso, M. M., Aloisio, A., Melchiorre, J., Giudice, M. L., & Marano, G. C. (2022). Size and shape optimization of a guyed mast structure under wind, ice and seismic loading. *Applied Sciences*, *12*(10). https://doi.org/10.3390/app12104875

[2] Sardone, L., Rosso, M. M., Cucuzza, R., Greco, R., & Marano, G. C. (2021). COMPUTATIONAL DESIGN OF COMPARATIVE MODELS AND GEOMETRICALLY CONSTRAINED OPTIMIZATION OF a MULTI DOMAIN VARIABLE SECTION BEAM BASED ON TIMOSHENKO MODEL. *14th International Conference on Evolutionary and Deterministic Methods for Design, Optimization and Control*. https://doi.org/10.7712/140121.7961.18535

[3] Cucuzza, R., Rosso, M. M., & Marano, G. (2021). Optimal preliminary design of variable section beams criterion. *SN Applied Sciences*, *3*. https://doi.org/10.1007/s42452-021-04702-5

[4] Cucuzza, R., Costi, C., Rosso, M. M., Domaneschi, M., Marano, G. C., & Masera, D. (0). Optimal strengthening by steel truss arches in prestressed girder bridges. *Proceedings of the Institution of Civil Engineers - Bridge Engineering*, *0*(0), 1–21. https://doi.org/10.1680/jbren.21.00056

[5] Fiore, A., Marano, G., Greco, R., & Mastromarino, E. (2016). Structural optimization of hollow-section steel trusses by differential evolution algorithm. *International Journal of Steel Structures*, *16*(2), 411–423. https://doi.org/10.1007/s13296-016-6013-1

[6] Marano, G., Trentadue, F., & Petrone, F. (2014). Optimal arch shape solution under static vertical loads. *Acta Mechanica*, *225*(3), 679–686. https://doi.org/10.1007/s00707-013-0985-0

[7] Melchiorre, J., Bertetto, A. M., & Marano, G. C. (2021). Application of a machine learning algorithm for the structural optimization of circular arches with different cross-sections. *Journal of Applied Mathematics and Physics*, *9*(5), 1159–1170.

[8] Marano, G. C., Trentadue, F., & Petrone, F. (2014). Optimal arch shape solution under static vertical loads. *Acta Mechanica*, *225*(3), 679–686.

[9] Di Trapani, F., Tomaselli, G., Sberna, A. P., Rosso, M. M., Marano, G. C., Cavaleri, L., & Bertagnoli, G. (2021). Dynamic response of infilled frames subject to accidental column losses. *International Conference of the European Association on Quality Control of Bridges and Structures*, 1100–1107.

[10] Aloisio, A., Pasca, D. P., Di Battista, L., Rosso, M. M., Cucuzza, R., Marano, G. C., & Alaggio, R. (2022). Indirect assessment of concrete resistance from fe model updating and young's modulus estimation of a multi-span psc viaduct: Experimental tests and validation. *Structures*, *37*, 686–697.

[11] Manuello, A. (2020a). Multi-body rope approach for grid shells: Form-finding and imperfection sensitivity. *Engineering Structures*, *221*, 111029.

[12] Fiore, A., Quaranta, G., Marano, G. C., & Monti, G. (2016). Evolutionary polynomial regression–based statistical determination of the shear capacity equation for reinforced concrete beams without stirrups. *Journal of Computing in Civil Engineering*, *30*(1), 04014111.

[13] Marano, G. C., Trentadue, F., & Greco, R. (2006). Optimum design criteria for elastic structures subject to random dynamic loads. *Engineering Optimization*, *38*(7), 853–871.

[14] Trentadue, F., Fiore, A., Greco, R., Marano, G. C., & Lagaros, N. D. (2020). Structural optimization of elastic circular arches and design criteria. *Procedia Manufacturing*, *44*, 425–432.

[15] Rosso, M. M., Cucuzza, R., Aloisio, A., & Marano, G. C. (2022). Enhanced multi-strategy particle swarm optimization for constrained problems with an evolutionary-strategies-based unfeasible local search operator. *Applied Sciences*, *12*(5), 2285.

[16] Trentadue, F., Marano, G. C., Vanzi, I., & Briseghella, B. (2018). Optimal arches shape for single-point-supported deck bridges. *Acta Mechanica*, *229*(5), 2291–2297.

[17] Halpern, A. B., & Adriaenssens, S. (2015). In-plane optimization of truss arch footbridges using stability and serviceability objective functions. *Structural and Multidisciplinary Optimization*, *51*(4), 971–985.

[18] Michiels, T., & Adriaenssens, S. (2018). Form-finding algorithm for masonry arches subjected to in-plane earthquake loading. *Computers & Structures*, *195*, 85–98.

[19] Marmo, F. (2021). Archlab: A matlab tool for the thrust line analysis of masonry arches. *Curved and Layered Structures*, *8*(1), 26–35.

[20] Rosso, M. M., Cucuzza, R., Di Trapani, F., & Marano, G. C. (2021). Nonpenalty machine learning constraint handling using pso-svm for structural optimization. *Advances in Civil Engineering*, *2021*.

[21] Zhou, Z., Wu, J., & Meng, S. (2014). Influence of member geometric imperfection on geometrically nonlinear buckling and seismic performance of suspen-dome structures. *International Journal of Structural Stability and Dynamics*, *14*(03), 1350070.

[22] Piana, G., Lofrano, E., Manuello, A., Ruta, G., & Carpinteri, A. (2017). Compressive buckling for symmetric twb with non-zero warping stiffness. *Engineering Structures*, *135*, 246–258.

[23] Bazzucchi, F., Manuello, A., & Carpinteri, A. (2017). Instability load evaluation of shallow imperfection-sensitive structures by form and interaction parameters. *European Journal of Mechanics-A/Solids*, *66*, 201–211.

[24] Manuello, A. (2020b). Semi-rigid connection in timber structure: Stiffness reduction and instability interaction. *International Journal of Structural Stability and Dynamics*, *20*(07), 2050072.

[25] Piana, G., Lofrano, E., Manuello, A., & Ruta, G. (2017). Natural frequencies and buckling of compressed non-symmetric thin-walled beams. *Thin-Walled Structures*, *111*, 189–196.

[26] Chen, Z., Xu, H., Zhao, Z., Yan, X., & Zhao, B. (2016). Investigations on the mechanical behavior of suspend-dome with semirigid joints. *Journal of Constructional Steel Research*, *122*, 14–24.

[27] Pelliciari, M., Marano, G. C., Cuoghi, T., Briseghella, B., Lavorato, D., & Tarantino, A. M. (2018). Parameter identification of degrading and pinched hysteretic systems using a modified bouc–wen model. *Structure and Infrastructure Engineering*, *14*(12), 1573–1585.

[28] Aloisio, A., Battista, L. D., Alaggio, R., Antonacci, E., & Fragiacomo, M. (2021). Assessment of structural interventions using bayesian updating and subspace-based fault detection methods:

The case study of s. maria di collemaggio basilica, l'aquila, italy. *Structure and infrastructure engineering*, *17*(2), 141–155.

[29] Aloisio, A., Di Battista, L., Alaggio, R., & Fragiacomo, M. (2020). Sensitivity analysis of subspace-based damage indicators under changes in ambient excitation covariance, severity and location of damage. *Engineering Structures*, *208*, 110235.

[30] Aloisio, A., Alaggio, R., Köhler, J., & Fragiacomo, M. (2020). Extension of generalized bouc-wen hysteresis modeling of wood joints and structural systems. *Journal of Engineering Mechanics*, *146*(3), 04020001.

[31] Aloisio, A., Pasca, D. P., Battista, L., Rosso, M. M., Cucuzza, R., Marano, G., & Alaggio, R. (2022). Indirect assessment of concrete resistance from fe model updating and young's modulus estimation of a multi-span psc viaduct: Experimental tests and validation. *Elsevier Structures*, *37*, 686–697. https://doi.org/10.1016/j.istruc.2022.01.045

[32] Marmo, F., & Rosati, L. (2012a). An improved flexibility-based nonlinear frame element endowed with the fiber-free formulation. *European Congress on Computational Methods in Applied Sciences and Engineering (ECCOMAS 2012). Viena, Austria*, 1–17.

[33] Marmo, F., & Rosati, L. (2012b). Analytical integration of elasto-plastic uniaxial constitutive laws over arbitrary sections. *International Journal for Numerical Methods in Engineering*, *91*(9), 990–1022.

[34] *MATLAB version 9.10.0.1649659 (R2021a) Update 1*. (2021).

[35] *SAP2000*. (2021).

[36] Carpinteri, A. (2013). *Structural mechanics fundamentals*. CRC Press.